Ab initio studies of phonon softening and high-pressure phase transitions of α-quartz SiO$_2$

N. Choudhury and S. L. Chaplot

Solid State Physics Division, Bhabha Atomic Research Centre, Trombay, Mumbai 400 085, India
(Received 6 November 2005; revised manuscript received 12 December 2005; published 22 March 2006)

Density functional perturbation theory calculations of α-quartz using extended norm conserving pseudopotentials have been used to study the elastic properties and phonon dispersion relations along various high symmetry directions as a function of bulk, uniaxial, and nonhydrostatic pressure. The computed equation of state, elastic constants, and phonon frequencies are found to be in good agreement with the available experimental data. A zone boundary (1/3, 1/3, 0) K-point phonon mode becomes soft for pressures above $P=32$ GPa. Around the same pressure, studies of the Born stability criteria reveal that the structure is mechanically unstable. The phonon and elastic softening are related to the high pressure phase transitions and amorphization of quartz, and these studies suggest that the mean transition pressure is lowered under nonhydrostatic conditions. The application of uniaxial pressure results in a post-quartz crystalline monoclinic $C2$ structural transition in the vicinity of the K-point instability. This structure, intermediate between quartz and stishovite has two-thirds of the silicon atoms in octahedral coordination while the remaining silicon atoms remain tetrahedrally coordinated. This monoclinic $C2$ polymorph of silica, which is found to be metastable under ambient conditions, is possibly one of the several competing dense forms of silica containing octahedrally coordinated silicon. The possible role of high pressure ferroelastic phases in causing pressure induced amorphization in silica are discussed.

PACS number(s): 63.20.Dj, 62.20.Dc, 63.70.+h, 31.15.Ar

I. INTRODUCTION

The silica polymorph quartz exhibits several interesting properties[1–17] including pressure induced amorphization,[1,2,8] high pressure and temperature phase transitions,[3,4,7,11–19] anomalous elastic properties,[3,6] negative Poisson ratios,[6(c)] soft mode behavior,[9,10,17] etc. Silica in its various crystalline and amorphous forms finds several industrial applications including being a raw material for glasses, ceramics, production of silicon, etc. Quartz oscillators and optical waveguides are used extensively in long distance telecommunications and industry. Despite its simple chemical composition, silica is known to assume various structures that have a wide range of densities (2.3–4.3 g/cm^3) and bulk modulii and has aroused considerable theoretical[7–26] and experimental[1,3–5,27–30] interest.

α-quartz is the most stable silica polymorph at ambient conditions (up to 3 GPa), and persists as a metastable state at higher pressures. Quartz amorphizes at pressures of around 18–35 GPa.[1–3] On the release of pressure, quartz remains amorphous,[1] but is anisotropic with the memory of the quartz crystallographic orientation.[6(a)] The atomic disorder with pressure was therefore believed to derive from small perturbations of the quartz structure. Although pressure induced amorphization occurs in a variety of solids like α-quartz,[1,2] coesite,[22] ice,[31] etc., its origins are not clearly understood. Several post-quartz crystalline phases have also been reported both from theory[7,12–14,16] and experiments.[1(b),4] First principles molecular dynamics simulations predicted a post-quartz trigonal structure for silica that results from annealing quartz at pressures near a major phonon instability.[7] The diffraction pattern of this phase compared favorably with that of an unidentified intermediate crystalline phase[1(b)] found in silica during the amorphization.

Molecular dynamics (MD) simulations using interatomic potentials fitted to first principles total energy surfaces[24,25] reveal pressure induced amorphization[8] at $P \sim 22$ GPa, in agreement with experiments. Around the amorphization pressure, α-quartz displays soft phonon modes[9,10] with a K-point phonon mode becoming unstable above $P=21$ GPa. First principles high pressure calculations, however, indicated that the K-point phonon instability occurs at a higher pressure.[17] Although the interatomic potentials[24–26] reproduce the observed pressure induced amorphization transition[9,10] pressure correctly, there are important differences in the computed elastic constants and Born stability criteria,[15] Raman and infrared data, as compared to experimental data[3,29,30] and available first principles results.[15,20]

We report density functional theory[32–38] (DFT) and density functional perturbation theory[32–38] (DFPT) calculations of the equation of state, elastic constants, Born stability criteria, phonon dispersion relations, and their variations with the pressure of α-quartz. Our goals are to (i) understand the K-point phonon instability and its variations under bulk and uniaxial compression as well as under nonhydrostatic conditions, (ii) study the high pressure phase transitions of quartz, and (iii) understand the mechanical stability of quartz at high pressure, as studied from the elastic constants and Born stability criteria. There are various controversies in the literature[3,16] on the appropriate Born stability criteria to be applied to study the mechanical stability of quartz at high pressure, etc. We address these issues, and have undertaken systematic high pressure studies of a variety of properties, including under nonhydrostatic conditions. A monoclinic high pressure crystalline post-quartz phase is obtained and its structural properties studied.
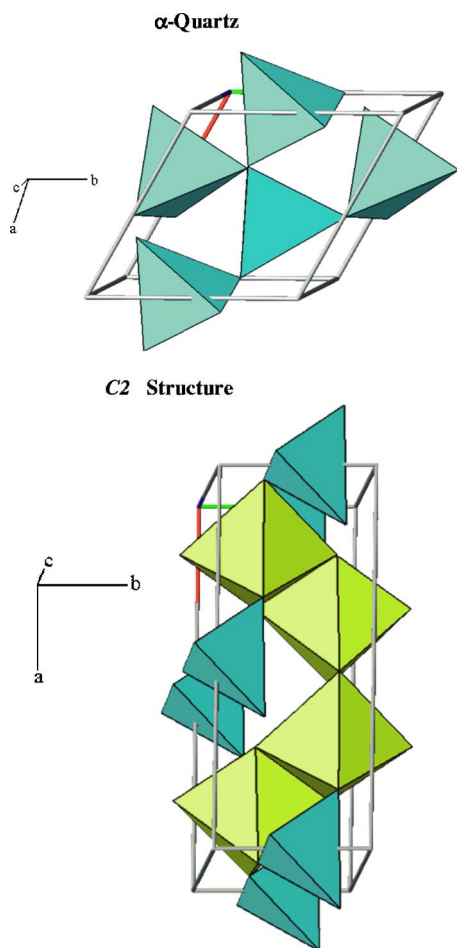
α-Quartz

C2 Structure

FIG. 1. (Color online). Polyhedral representation of the computed α-quartz and the high pressure C2 structure obtained using the software xtaldraw (Ref. 52). The crystallographically distinct silicon atoms are shown with different shades.

II. TECHNIQUES

Quartz has a trigonal structure[28(e)] (space group $P3_221$) with 9 atoms/unit cell. Density functional perturbation theory (DFPT) linear response calculations with a plane-wave basis set, as implemented in the code ABINIT,[39] were undertaken. We used the local density approximation (LDA) involving a rational polynomial parametrization of the exchange-correlation functional[40] based on Ceperley and Alder[41] electron-gas data and employ well tested extended norm conserving separable pseudopotentials[42] used earlier for zero pressure calculations of α-quartz[20] and stishovite.[21] The computed phonon frequencies and LO-TO splittings,[20(a),21] dispersion relations,[20(b),21] density of states[20(c)] specific heat,[20(c)] and mean square atomic displacements[20(c)] using these pseudopotentials were found to be in good agreement with experiments. A large plane wave energy cutoff of 120 Ry and smearing of 1 Ry were used to obtain precise values of the stress tensor in the high pressure studies. The Brillouin zone (BZ) integrations were performed using a 4 × 4 × 4 special **k**-point mesh. Selected computations of the long wavelength and zone boundary K-point phonons with a 6 × 6 × 6 special k-point mesh showed that the 4 × 4 × 4
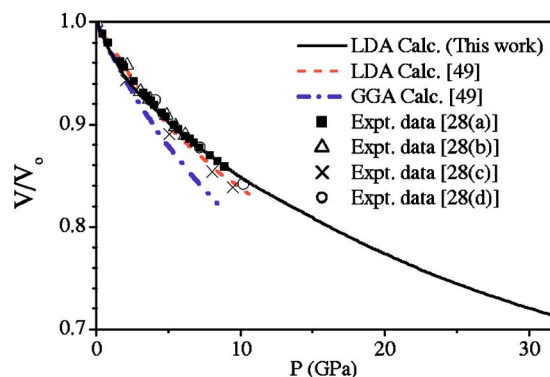

FIG. 2. (Color online) A comparison of the calculated (full line) equation of state of α-quartz with reported LDA and GGA calculations (Ref. 49) and experimental data (Refs. 28) (symbols).

mesh was sufficient and the total energies, structural variables, and phonon frequencies were well converged at the highest pressures. At each pressure, the structures were completely relaxed prior to the calculations.

To obtain the phonon frequencies at a general wave vector, we first computed the dynamical matrices on the (4, 4, 4) wave vector grid involving 10 wave vectors in reciprocal space, and computed the interatomic force constants. The long-range dipole-dipole interactions were taken into account separately using the calculated anisotropic Born effective charge tensor and dielectric tensor. The elastic constants as a function of pressure were evaluated both from DFPT linear response[38] using a 6 × 6 × 6 special **k**-point mesh with
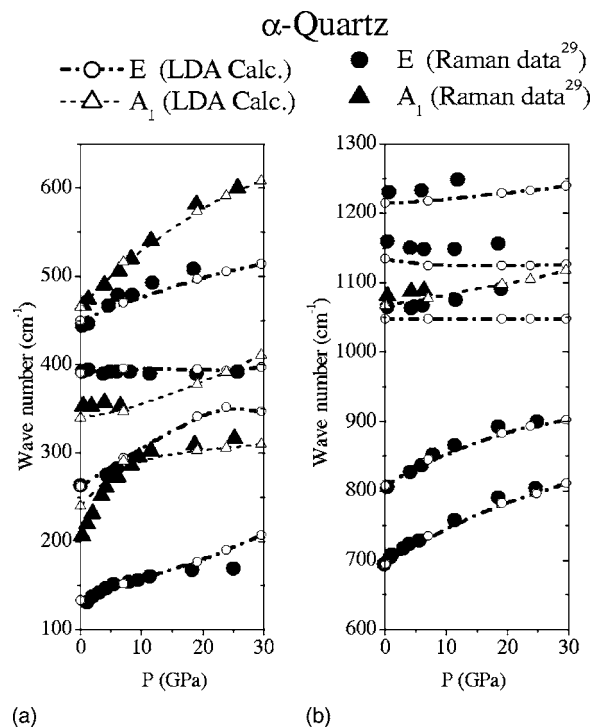

FIG. 3. A comparison of the computed (open symbols and lines) and experimental (Ref. 29) (filled symbols) long wavelength phonon frequencies as a function of hydrostatic pressure. The group theoretical phonon mode assignments are indicated.

TABLE I. Stable and metastable quartz structures as a function of pressure obtained from symmetry preserving structural relaxations with space group $P3_221$. The Si atoms are in $3b$ Wyckoff positions with fractional coordinates $(u,0,1/6)$, $(0,u,5/6)$, $(-u,-u,1/2)$ and the O atoms in $6c$ positions with coordinates (x,y,z) $(-y,x-y,z+2/3)$ $(-x+y,-x,z+1/3)$ $(y,x,-z)$ $(x-y,-y,-z+1/3)$ $(-x,-x+y,-z+2/3)$. P1, P2, and P3 represent nonhydrostatic pressures with stress tensor $\sigma_{xx}=\sigma_{yy}=-19$ GPa, $\sigma_{xy}=\sigma_{yz}=\sigma_{zy}=0$ and $\sigma_{zz}=-24.8, -29.6$ and -38 GPa, respectively. $Pc1$ has the stress tensor $\sigma_{xx}=\sigma_{yy}=-1.1$ GPa, $\sigma_{xy}=\sigma_{yz}=\sigma_{zx}=0$ and $\sigma_{zz}=-6.9$ GPa. All these structures are dynamically stable in the entire Brillouin zone.

P (GPa)	a (Å)	c (Å)	u	x	y	z
Bulk pressure						
0.24	4.8137	5.3150	0.4613	0.4097	0.2814	0.2748
7.1	4.5795	5.1908	0.4451	0.3964	0.3048	0.2589
19.1	4.3444	5.0881	0.4311	0.3773	0.3208	0.2513
23.7	4.2773	5.0584	0.4271	0.3708	0.3247	0.2501
29.6	4.2057	5.0229	0.4227	0.3633	0.3286	0.2491
Nonhydrostatic pressure						
P1	4.3825	4.9724	0.4286	0.3780	0.3203	0.2494
P2	4.4135	4.8887	0.4271	0.3788	0.3193	0.2484
P3	4.4813	4.7386	0.4258	0.3809	0.3161	0.2468
Pc1	4.8316	5.0438	0.4546	0.4070	0.2879	0.2646

an energy cutoff of 120 Ry as well as directly from the stress-strain relations.[43,44] To compute the elastic constants under pressure, we applied appropriate strains that yield the various elastic constants and computed the total energies and stresses, after careful relaxation of the strained structures. Linear response DFPT studies with strain perturbations using the reduced coordinate metric tensor method of Hamann *et al.*[38] were also used to study the elastic constants at high pressure. The linear response results give the proper elastic constant tensors[38] and appropriate pressure corrections[38,45–47] were applied to obtain the stiffness constants that satisfy the Born stability criteria.

III. RESULTS

A. Equation of state and long wavelength phonon frequencies

The computed crystal structure, equation of state, and long wavelength phonon frequencies (Figs. 1–3) are found to be in good agreement with reported high pressure experimental data[28,29] and available first principles LDA calculations.[20,48–50] First principles LDA[48–50] and Generalized Gradient Approximation (GGA)[49,50] studies of the equation-of-state of α-quartz have been reported by various workers,[48–50] and we have compared our calculated results with the theoretical[49] and reported experimental[28] studies in Fig. 2. Quartz has a framework structure (Fig. 1) formed by corner shared silicate tetrahedral units. The application of pressure distorts and causes tilts in the tetrahedral units and quartz reconstructively transforms successively to the coesite and octahedrally coordinated stishovite phases at high pressure. Due to large kinetic barriers, quartz, however, persists as a metastable state up to very high pressures at room temperature. The four to six coordinated silicon transition is known to cause seismic discontinuities in the Earth's mantle, which marks the transition from the upper to the lower mantle, and understanding the mechanism of this transition particularly for a model system like silica is particularly useful. Hamann's studies[50] on the quartz to stishovite phase transition indicates that only the GGA yields correct relative energies and leads to a reasonably accurate prediction of the transition pressure. However the structural parameters within the GGA are less accurately predicted;[50] these have motivated the development of more accurate GGA.[51] The LDA calculations[48–50] of α-quartz predict the equilibrium volume with an accuracy of 1%, whereas the GGA[49,50] lead to an overestimate of 6.6%. The LDA also lead to a consistently more accurate description of all atomic coordinates;[48,50] we have therefore adopted the LDA for our high pressure studies. Even within the LDA, the reported bulk modulii show a large scatter (35 GPa,[49] 45 GPa,[50] both having $B'=4.9$; $B=38.1$ GPa[48]); the corresponding equilibrium LDA volumes[48–50] typically scatter between 35.8 and 38.55 Å³. Experimental synchrotron x-ray diffraction measurements of Haines *et al.*,[4] indicate that quartz is metastable upto much higher pressures than the reported equation-of-state

TABLE II. Variations of the dynamic Born effective charge tensors of the Si and O atoms with pressure. Only the tensors of the inequivalent atoms are listed. The charge tensors of other atoms can be derived from symmetry. x and z are, respectively, along the a and c axes.

	P (GPa)	Z^*_{xx}	Z^*_{yy}	Z^*_{zz}	Z^*_{xy}	Z^*_{xz}	Z^*_{yx}	Z^*_{yz}	Z^*_{zx}	Z^*_{zy}
Si	0.24	3.01	3.63	3.45	0	0	0	0.28	0	−0.32
O	0.24	−1.32	−2.00	−1.72	0.42	0.22	0.48	−0.71	0.29	−0.66
Si	19.1	3.17	3.53	3.53	0	0	0	0.26	0	−0.32
O	19.1	−1.39	−1.96	−1.76	0.31	0.043	0.36	−0.56	0.11	−0.48
Si	29.6	3.25	3.56	3.58	0	0	0	0.21	0	−0.31
O	29.6	−1.43	−1.97	−1.79	0.28	0.00	0.33	−0.51	0.05	−0.42
Si	38.4	3.31	3.61	3.63	0	0	0	0.16	0	−0.30
O	38.4	−1.57	−1.99	−1.81	0.27	−0.02	0.31	−0.48	0.01	−0.38

TABLE III. The computed electronic (ε^∞) and zero frequency (ε^0) dielectric tensors as function of bulk pressure. z and x are, respectively, along and perpendicular to the c axis.

	$P=0.24$ GPa	$P=7$ GPa	$P=19$ GPa	$P=24$ GPa	$P=30$ GPa
ε_{xx}^∞	2.53	2.71	2.90	2.97	3.04
ε_{zz}^∞	2.56	2.75	2.95	3.01	3.08
ε_{xx}^0	4.766	5.19	5.87	6.16	6.55
ε_{zz}^0	4.967	5.37	6.03	6.31	6.70

measurements[28] that are typically available in the 0–10 GPa range; in the present study, we report the equation-of-state over the entire pressure range (0–32 GPa), over which α-quartz is dynamically and mechanically stable (Fig. 2).

The long wavelength phonon modes in α-quartz at the zone center Γ point can be classified as

$$\Gamma: 4A_1 + 5A_2 + 9E.$$

The E phonon modes are doubly degenerate polar phonon modes. The computed structures and variations of the Born effective charge tensors, electronic dielectric tensors, and phonon frequencies with pressure are given in Tables I–IV. All the structures given in Table I are dynamically stable in the entire Brillouin zone and represent stable and metastable high pressure quartz structures under hydrostatic and nonhydrostatic conditions. Both the Born effective charges (Table II) and electronic dielectric tensors (Table III) are required to understand the influence of the macroscopic electric field on long wavelength phonon properties. The Born effective charge tensor gives a measure of the local dipole moment that develops when the nuclei are moved and corresponds to the variation of the polarization with atomic displacements. As the Born effective charge tensor $\mathbf{Z}_{\alpha\beta}^*(k)$ is a mixed second derivative of the total energy, with respect to macroscopic electric field component E_α and atomic displacement component $\tau_{k,\beta}$, there is no requirement that the tensor be symmetric. The pressure variations of the low and high frequency dielectric tensors are given in Table III. The zero pressure dielectric tensors are overestimated, as is typical within the LDA; however, the application of the scissors correction[20(a)] has been found to improve the agreement with experimental data for both high and low frequency tensors. Gonze et al.[20(a)] discuss the important role of the anisotropy of the Born effective charge tensors in describing the observed zero pressure LO-TO splittings in α-quartz. Our zero pressure results (Table IV) are in complete agreement with their studies.[20(a)] At higher pressures, the anisotropy of the charge tensor (Table II) is found to significantly reduce, which indicates important changes in the bonding character. The LO-TO splittings of the A_2 phonon modes (with macroscopic electric field parallel to the c axis), especially the 343 and 763 cm^{-1} phonon modes, significantly increase with pressure. The splittings of the doubly degenerate E phonon modes that have their macroscopic electric field perpendicular to the c axis are not largely altered by pressure with the simultaneous hardening of both the LO and TO modes. The 465 cm^{-1} nonpolar A_1 phonon mode (Table V) hardens significantly with pressure in good agreement with experimental measurements.[29]

B. High pressure elastic constants and Born stability criteria

The computed $P=0$ elastic constants obtained from linear response DFPT calculations are in good agreement with reported experimental data (Table VI). We have compared our

TABLE IV. The computed long wavelength longitudinal optic (LO) and transverse optic (TO) phonon frequencies (cm^{-1}) and LO-TO splittings ($\Delta\omega = \omega_{LO} - \omega_{TO}$) of α-quartz at selected bulk pressures. The group theoretical mode assignments are indicated. The E (A_2) phonon modes are polar with a macroscopic electric field perpendicular (parallel) to the c axis, respectively.

$P=0.24$ GPa ω_{TO}	$P=0.24$ GPa ω_{LO}	$P=0.24$ GPa $\Delta\omega$	$P=7$ GPa ω_{TO}	$P=7$ GPa ω_{LO}	$P=7$ GPa $\Delta\omega$	$P=19$ GPa ω_{TO}	$P=19$ GPa ω_{LO}	$P=19$ GPa $\Delta\omega$	$P=24$ GPa ω_{TO}	$P=24$ GPa ω_{LO}	$P=24$ GPa $\Delta\omega$	$P=30$ GPa ω_{TO}	$P=30$ GPa ω_{LO}	$P=30$ GPa $\Delta\omega$
E														
133	134	1	152	152	0	172	177	5	190	190	0	207	207	0
263	265	2	294	298	4	341	349	8	352	366	14	347	380	33
379	390	11	377	396	19	367	395	28	368	393	25	385	397	12
445	500	55	470	520	50	497	544	47	505	552	47	514	562	48
694	698	4	735	742	7	782	790	8	796	805	9	811	821	10
795	807	12	834	845	11	876	883	7	888	893	5	899	902	3
1050	1214	164	1049	1217	168	1048	1229	181	1048	1233	185	1047	1239	192
1134	1129		1124	1116		1125	1112		1125	1112		1126	1125	
A_2														
343	368	25	334	363	29	334	373	39	336	379	43	337	387	50
495	542	47	523	552	29	539	550	11	541	547	6	541	543	2
765	787	22	770	820	50	774	857	83	776	868	92	780	882	102
1063	1223	160	1080	1235	155	1103	1253	150	1110	1257	147	1116	1262	146

TABLE V. The computed long wavelength nonpolar A_1 phonon frequencies (cm^{-1}) of α-quartz at selected bulk pressures.

$P=0.24$ GPa	$P=7$ GPa	$P=19$ GPa	$P=24$ GPa	$P=30$ GPa
ω	ω	ω	ω	ω
239	291	303	306	310
340	346	378	392	411
465	516	574	591	608
1068	1077	1098	1105	1118

zero pressure elastic constants with the calculated LDA results of Holm and Ahuja;[18] although the overall agreements with experiments seem similar, the calculated individual elastic constants obtained have some differences (Table VI). The elastic constants of α-quartz, particularly the soft elastic constants C_{12}, C_{13}, and C_{14}, are very sensitive to the relaxed structural parameters obtained. While we obtain better agreement with experiments for C_{13} and C_{14}, Holm and Ahuja[18] obtain better agreement for C_{11} and C_{12}. It is interesting to see that even in the experiments, the C_{33} values reported[3(a),5] (Table VI) are different; a somewhat large scatter is also obtained in the bulk modulii and observed equation of state.[28]

There are various definitions of the elastic constants;[38,43,45–47] however, the elastic constant obtained from stress-strain relations and from long-wavelength lattice dynamics are different[43,45–47] for nonzero stresses. The elastic constants that define the mechanical stability criteria under pressure are those appearing in stress-strain relations.[45–47] The linear response formulation[32] taking into account strain perturbations, on the other hand, gives the "proper elastic constant tensor."[38] While these two definitions become identical at zero pressure, under hydrostatic pressure appropriate pressure corrections have to be applied[38,45–47] to the linear response results.

The computed high pressure elastic constants of α-quartz evaluated for bulk hydrostatic pressure using the stress-strain relations are compared with reported high pressure Brillouin scattering measurements[3(a)] in Fig. 4. The computed elastic constants obtained from linear response studies with strain perturbations and appropriate pressure corrections[38,45–47] are found to be in excellent agreement (to well within 0.5 GPa)

TABLE VI. Zero pressure elastic constants (GPa) of α-quartz ($^*C_{12}=C_{11}-2C_{66}$).

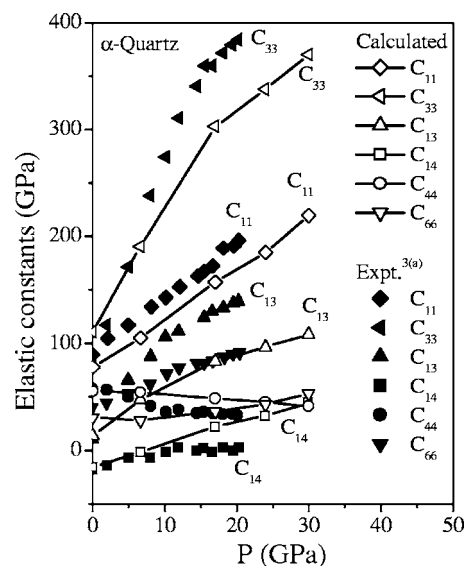| Elastic constants	LDA calculations This work	LDA calculations Ref. 18	Experimental Ref. 5	Experimental Ref. 3(a)
C_{11}	78.1	90	86.8	85.9
C_{12}^*	16.0	12	7.04	7.16
C_{13}	13.9	21	11.91	10.94
C_{14}	−15.7	−12	−18.04	−17.66
C_{33}	110.8	97	105.75	89.59
C_{44}	55.2	61	58.2	57.66

FIG. 4. A comparison of the computed elastic constants as a function of pressure with the reported Brillouin scattering single crystal experimental data of Gregoryanz *et al.* [Ref. 3(a)].

with the values obtained from stress-strain relations. The elastic constants C_{11} and C_{33} increase sharply with pressure. Although the zero pressure elastic constants are in good agreement with experiments (Table VI), the computed high pressure average elastic constants seem underestimated (Fig. 4). The elastic constants of α-quartz are found to be quite sensitive to the hydrostatic pressure conditions, and the variations could perhaps be due to the difficulties in maintaining perfect hydrostatic conditions at high pressure in the experiments.

The mechanical Born stability criteria for trigonal structures results in various constraints for the elastic constants, which are given by[3,11,15]

$$B_1 = C_{11} - |C_{12}| > 0,$$

$$B_2 = (C_{11} + C_{12})C_{33} - 2(C_{13})^2 > 0,$$

$$B_3 = (C_{11} - C_{12})C_{44} - 2(C_{14})^2 > 0. \tag{1}$$

The computed variations of B_1, B_2, and B_3 with pressure are shown in Fig. 5. All the three conditions given in Eq. (1) must be simultaneously satisfied for the system to be mechanically stable.[11,15] B_1 and B_2 are positive up to 40 GPa (Fig. 5). The quartz structure becomes mechanically unstable around $P=32$ GPa, as B_3 becomes negative and the Born stability criteria gets violated. Our computed results and trends for B_1, B_2, and B_3 (Fig. 5) are in good qualitative agreement with the reported experimental Brillouin scattering results of Gregoryanz *et al.*[3(a)] and the theoretical studies of Bingelli *et al.*[15] While the interatomic potentials yield lower transition pressures[15] of around $P=20$ GPa, the first principles results reveal that the system is mechanically unstable at pressures of around $P=32$ GPa.
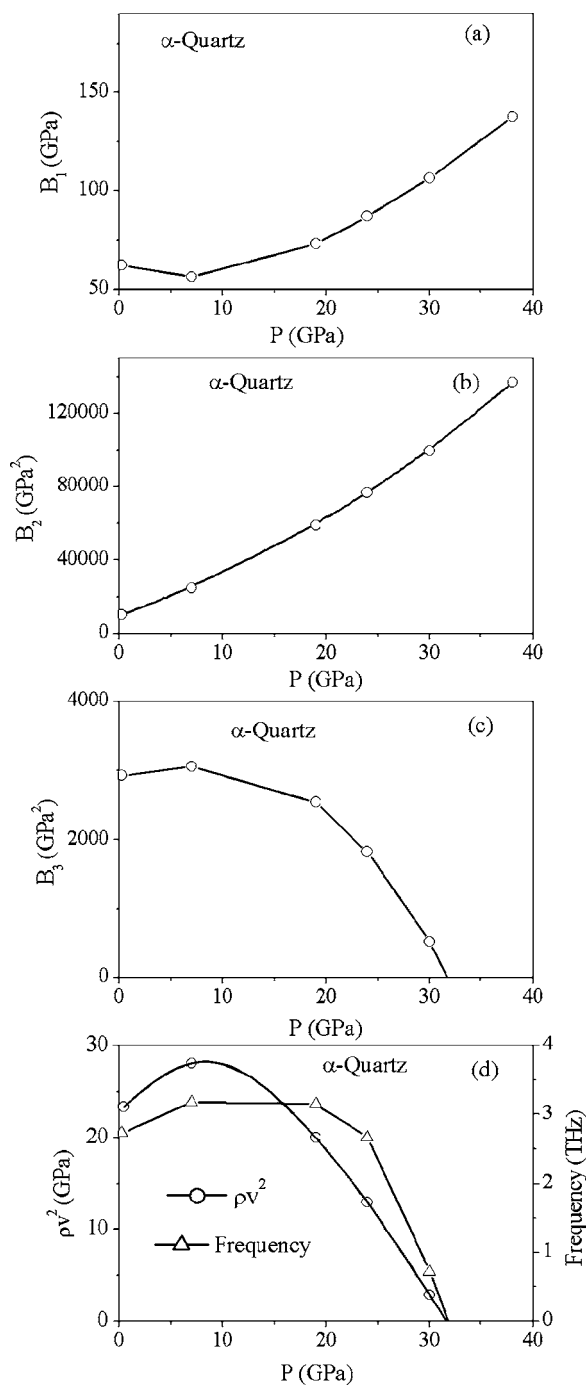
FIG. 5. The variations of the computed B_1, B_2, and B_3, and the soft acoustic mode elastic constant ρv^2 with pressure. B_3 and ρv^2 are negative above $P \sim 32$ GPa, which indicates the onset of mechanical instability in α-quartz at high pressure. In (d), we also display the variation of the calculated soft mode K-point phonon frequency with pressure.

C. High pressure phonon instabilities and structural phase transitions

The computed phonon dispersion relations in α-quartz at various bulk pressures, namely, $P=0$, 24, 30, and 38 GPa are shown in Fig. 6. Almost all the zone center Raman and infrared modes harden with pressure, as observed experimen-

tally (Fig. 3). The zero pressure phonon dispersion reveals a large bandgap from 24–31 THz; this gap significantly lowers at high pressures. The lowest zone boundary K-point phonon mode becomes soft for bulk pressures above $P=32$ GPa and the pressure evolution of the phonon instability can be clearly seen from Figs. 5 and 6. At $P=24$ GPa, the K-point lowest phonon mode is quite stable; the onset of the instability occurs well above this pressure.

We have also computed the "elastic constant" corresponding to the soft acoustic mode using the relation[3(a)]

$$\rho v^2 = \frac{1}{4}\{(C_{11} - C_{12} + 2C_{44})$$

$$- [(C_{11} - C_{12} - 2C_{44})^2 + 16C_{14}^2]^{1/2}\}. \quad (2)$$

For small B_3, $\rho v^2 = B_3 C_{44}/2[C_{14}^2 + C_{44}^2]$, which is found to be proportional to B_3. The computed ρv^2 (Fig. 5) goes through a maximum near 6.5 GPa and then decreases linearly, vanishing at high pressures. Similar trends have been noticed from Brillouin scattering measurements[3(a)] and have been associated with the proper ferroelastic behavior in the high pressure regime.[3(a)] The phase transition pressure obtained from the vanishing "elastic constant" ρv^2 (Fig. 5(d)) and K-point phonon frequency (Fig. 5(d)) are very close ($P \sim 32$ GPa). The transition pressure predicted from first principles studies ($P=32$ GPa) is higher than that obtained from interatomic potentials ($P=21$ GPa[9] using the Tsuneyuki et al. potentials,[24] $P=27$ GPa[10] using other potentials) and in good agreement with the LDA calculations of Baroni and Giannozzi[17] giving the K-point instability at $P \sim 32$ GPa. The mechanical instability of the quartz structure obtained from the Born stability criteria B_3 occurs in the vicinity of the K-point instability, both using interatomic potentials[15] and from first principles studies.

In Fig. 6, we also display the phonon dispersion for various nonhydrostatic situations. While the plot in Fig. 6(e) with nonhydrostatic pressure involving high pressure along the c axis as well as the ab plane has a dispersion similar to that under hydrostatic situations, there is a drastic change in dispersion for compression only along the c axis (Fig. 6(f)). On the gradual application of uniaxial pressure, phonon softening is found for the stress tensor $\sigma_{xx} = \sigma_{yy} = 0$, $\sigma_{zz} = -15.8$ GPa, $\sigma_{zx} = \sigma_{xy} = \sigma_{yz} = 0$. The phonon softening is related to the high pressure phase transitions and amorphization of quartz[9,10] and these results suggest that the mean transition pressure is significantly lowered under nonhydrostatic conditions. This possibly explains the wide range of amorphization pressure (18–35 GPa) obtained in the experiments.[1–3] The nature of phonon dispersion (Fig. 6(f)) along the Γ-A direction is quite different for uniaxial compression along the c axis.

Unconstrained structural relaxation of the 9-atom unit cell of α-quartz around this stress tensor $\sigma_{xx} = \sigma_{yy} = 0$, $\sigma_{zz} = -15.8$ GPa, $\sigma_{zx} = \sigma_{xy} = \sigma_{yz} = 0$ yields a post-quartz transition to a crystalline monoclinic $C2$ structure. Gradual symmetry preserving structural relaxation yields the corresponding monoclinic $C2$ structure for bulk pressures. The $C2$ structure has a significantly lower volume that results in a lower enthalpy (which gives the zero temperature free en-
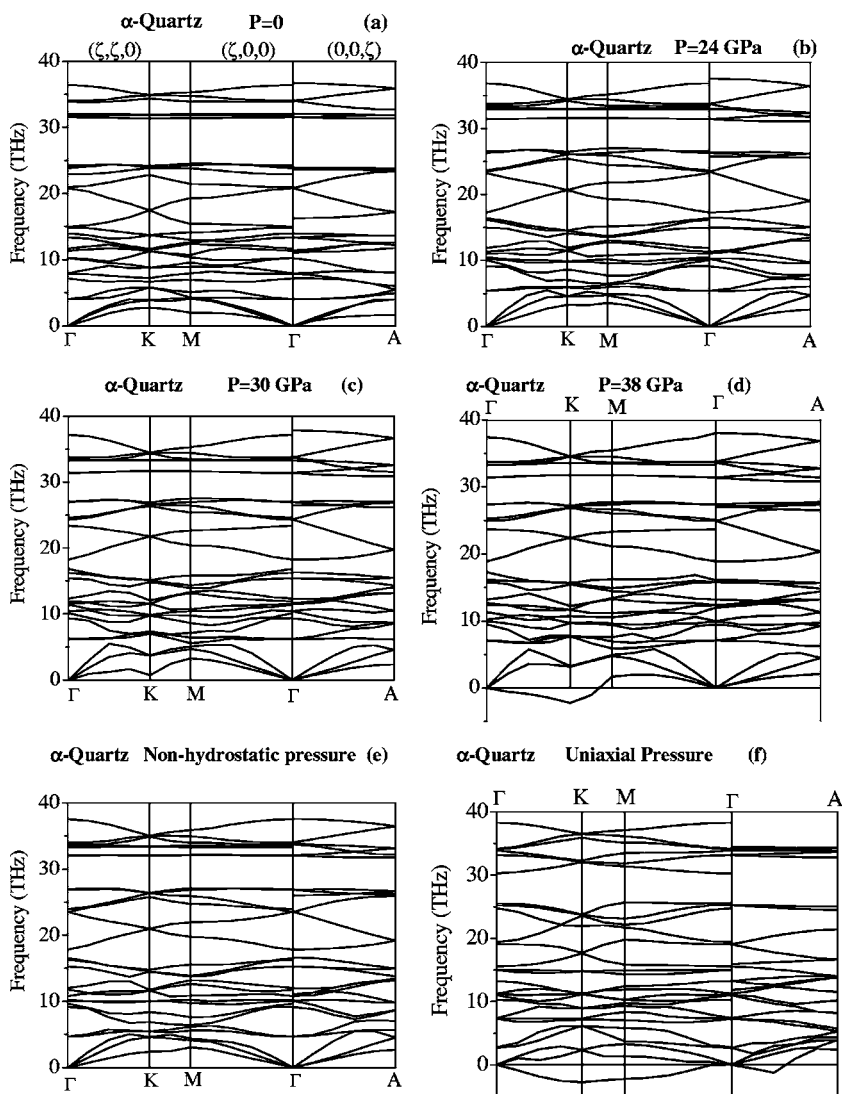
FIG. 6. The computed high pressure phonon dispersion relations of α-quartz. While Γ is the zone center point, K, M, and A are zone boundary points in the Brillouin zone (Ref. 9). The wave vector directions are as indicated on the top of the figure in (a). At high pressures, the lowest phonon mode at the K-point becomes unstable. While (a), (b), (c), and (d) give the phonon dispersion of α-quartz for bulk hydrostatic pressures, (e) corresponds to the nonhydrostatic situation with $\sigma_{xx}=\sigma_{yy}=-19$ GPa, $\sigma_{xy}=\sigma_{yz}=\sigma_{zx}=0$, and $\sigma_{zz}=-29.6$ GPa. (f) has the stress tensor $\sigma_{xx}=\sigma_{yy}=0$ GPa, $\sigma_{xy}=\sigma_{yz}=\sigma_{zx}=0$, and $\sigma_{zz}=-15.8$ GPa.

ergy, neglecting zero-point vibrational contributions) than the α-quartz structure for bulk pressures of above $P=9$ GPa (Fig. 7). Two-thirds of the silicon atoms are in octahedral coordination in the $C2$ structure (Table VII), while the remaining one-thirds silicon are tetrahedrally coordinated both under uniaxial and bulk pressure conditions. The $C2$ structure has edge-shared octahedral units with corner-shared silicate tetrahedra which form a framework structure (Fig. 1).

The computed x-ray diffraction patterns and d spacings of the post-quartz monoclinic $C2$ structure at $P=38$ GPa have been studied (Table VIII). The largest intensities in the $C2$ structure occurs for d spacings (Å) of 4.7944 (19.5), 3.6912 (14.5), 3.0573(26.7), 2.7505 (50), 2.6045 (64.8), 2.4478 (31.4), 1.8456 (39.67), 1.7819 (33.35), and 1.6642 (30.91), where the numerical values in parentheses give the relative intensities. The computed x-ray intensities of the high pressure $C2$ structure are compared with experimental synchrotron x-ray diffraction data (Fig. 8) for the observed high pressure post-quartz crystalline phases.[1(b),4] Haines *et al.*[4] obtained a post-quartz crystalline phase by compressing quartz to 45 GPa at room temperature in a close to hydrostatic, helium pressure medium. Kingma *et al.*[1(b)] have reported the

energy-dispersive diffraction spectra of a post-quartz crystalline phase obtained by the quasihydrostatic compression of polycrystalline α-quartz. The computed diffraction patterns (Fig. 8) and d spacings (Table VIII) of the $C2$ structure are
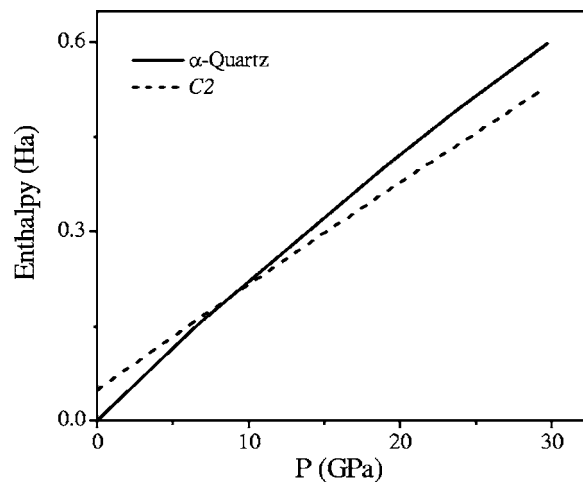

FIG. 7. The computed enthalpy of α-quartz and the $C2$ structure as a function of pressure.

TABLE VII. The computed unit cell constants and Si-O bond lengths in the monoclinic $C2$ structure. The fractional coordinates x, y, and z of the Si and O atoms in the asymmetric unit cell are listed. The Si1 silicon atoms are tetrahedrally coordinated, while the two equivalent Si2 atoms are in octahedral coordination; bond-length numbers in parentheses represent the multiplicity. The zero pressure $C2$ structure is metastable and has a higher free energy than the α-quartz structure. P^* represents the structure under uniaxial pressure conditions with stress tensor $\sigma_{xx}=\sigma_{yy}=0$ GPa, $\sigma_{xy}=\sigma_{yz}=\sigma_{zx}=0$ and $\sigma_{zz}=-16$ GPa.

	$P=0$ GPa	$P=8.8$ GPa	$P=38$ GPa	P^* GPa
a (Å)	8.5527	8.4691	8.2318	8.6327
b (Å)	3.4566	3.4200	3.3285	3.5142
c (Å)	5.375	5.2940	5.1040	5.1578
β	109.261	109.852	110.060	111.054
Si1 (x,y,z)	0, 0.5414, 0	0, 0.5423, 0	0, 0.5460, 0	0, 0.5548, 0
Si2 (x,y,z)	0.1797, 0.3086, 0.6240	0.1774, 0.30818, 0.62029	0.1754, 0.3065, 0.6192	0.1762, 0.3068, 0.6157
O (x,y,z)	0.9897, 0.3212, 0.2734	0.9928, 0.3175, 0.2758	0.9975, 0.3081, 0.2768	0.9931, 0.3172, 0.2756
O (x,y,z)	0.8106, 0.8084, 0.4279	0.8123, 0.8082, 0.4277	0.8160, 0.8070, 0.4268	0.8099, 0.8063, 0.4246
O (x,y,z)	0.1647, 0.7943, 0.0924	0.1656, 0.7982, 0.0893	0.1671, 0.8086, 0.08114	0.1654, 0.7955, 0.0841
Si(1)-O (Å)	1.6831(2), 1.5915(2)	1.6694(2), 1.5832 (2)	1.6258(2), 1.5611(2)	1.6682(2), 1.5805(2)
Si(2)-O (Å)	1.6614, 1.7116, 1.7562, 1.7578, 1.7730, 2.0425	1.6564, 1.7087, 1.7352, 1.7354, 1.7712, 1.9584	1.6312, 1.6809, 1.6836, 1.6875, 1.7559, 1.8555	1.6573, 1.7434, 1.7662, 1.7768, 1.7802, 1.8936

overall in fair agreement with the synchrotron x-ray data of Haines *et al.*,[4] which have been indexed based on a low symmetry $P2_1/c$ monoclinic structure.[4] While we obtain diffraction peaks and d spacings around the positions indicated by Kingma *et al.*,[1(b)] the $C2$ structure has more peaks (Table VIII, Fig. 8) and lower symmetry than their reported post-quartz crystalline phase.[1(b)]

Although the monoclinic $C2$ structure has a lower free energy for pressures above $P=9$ GPa (Fig. 7), quartz can persist metastably up to the point of onset of elastic and dynamical instability, which occurs around bulk pressures of $P=32$ GPa (Fig. 7). This monoclinic $C2$ monoclinic polymorph of silica, which is found to be metastable under ambient conditions, is possibly one of the several competing[23] dense forms of silica containing octahedrally coordinated silicon. It is interesting to note that the zero pressure metastable $C2$ quenched structure obtained from our studies has two-thirds of the silicon atoms, which are 5 coordinated to within 1.8 Å, with a sixth oxygen at 2.04 Å. The longest Si-O bond is quite compressible, and with increasing bulk pressure, the octahedral distortions in the $C2$ structure are lowered.

IV. DISCUSSION

First principles calculations have revealed that the energy landscape in silica at high pressure is quite complex and there are several possible octahedrally coordinated competing dense high pressure silica structures.[23] The crystalline high pressure structures obtained seems to depend on the kinetics and the pathway adopted and several post-quartz crystalline structures have been reported both from theory[7,12,14,16] and experiments.[1(b),4] Haines *et al.*[4] have indexed the diffraction patterns for their observed high pressure crystalline post-quartz phase based on a monoclinic cell with space group $P2_1/c$, with a model structure built up of

TABLE VIII. Comparisons of the computed d spacings in the computed $C2$ structure with the reported d spacings in the observed post-quartz structures of Haines *et al.* (Ref. 4) and Kingma *et al.* [Ref. 1(b)].

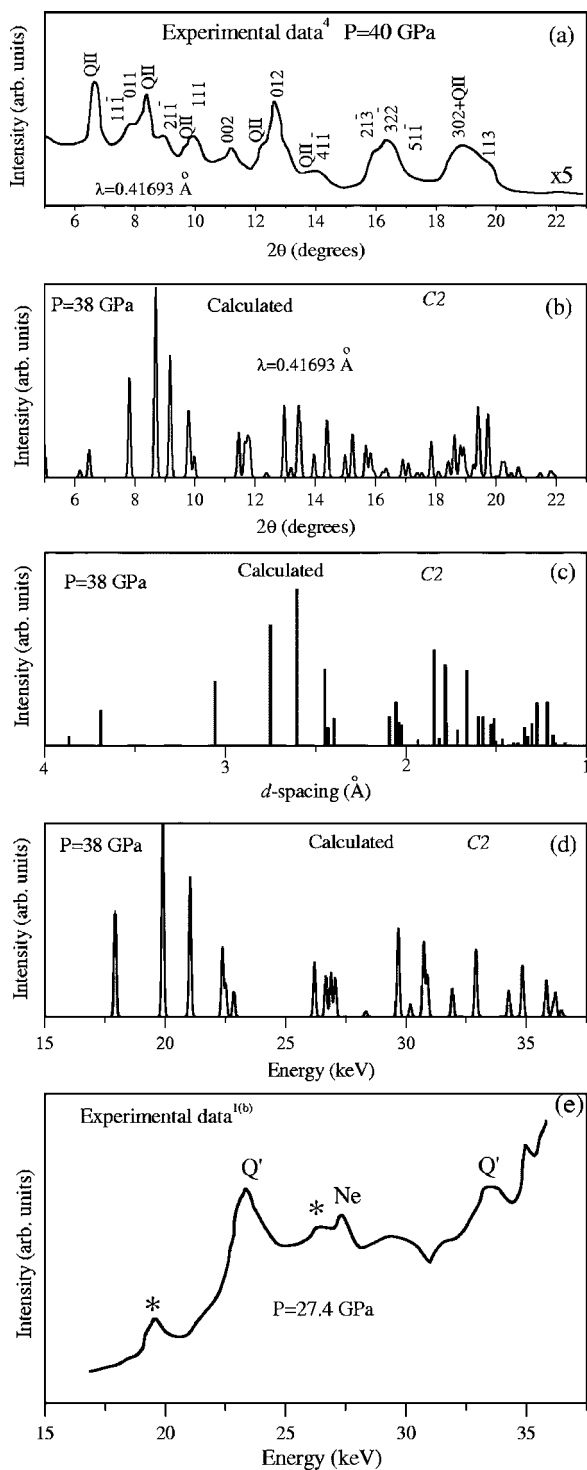| $C2$ structure $(P=38$ GPa) d spacing (Å)	Post-quartz structure of Haines *et al.* (Ref. 4) d spacing (Å)	Post-quartz structure of Kingma *et al.* [Ref. 1(b)] d spacing (Å)
4.794		
3.867		3.776
3.691	3.603	3.613
3.057	3.161, 2.976	3.027
2.751	2.745	2.668
2.605		
2.448	2.48	
2.397	2.225	
2.091	2.175	2.129
2.024	1.968	
1.846	1.926	
1.782		
1.716	1.725	
1.665		
1.572	1.546	
1.529	1.517	
1.513	1.492	
1.344	1.413	
1.302	1.305	
1.275	1.278	
1.275	1.258	
1.216	1.236	
1.188	1.191	
1.171	1.169	

FIG. 8. A comparison of the observed x-ray diffraction intensities (Ref. 4) in the reported ($\lambda = 0.41693$ Å) post-quartz phase of Haines *et al.* (Ref. 4) (a) with the computed x-ray intensities in the *C*2 structure (b). Peaks labeled QII in (a) correspond to post-quartz peaks. The calculated *d* spacing and energy dispersive spectra of the *C*2 structure (c)–(d) are compared with the reported synchrotron energy-dispersive x-ray diffraction pattern (e) in the post-quartz phase crystalline phase of Kingma *et al.* [Ref. 1(b)]. In (e), * represents post-quartz phase peaks, *Q'* are shifted quartzlike diffraction peaks, and Ne has been identified as diffraction lines of the pressure transmitting medium neon [Ref. 1(b)].

$3 \times 3 \times 2$ zigzag chains of SiO_6 octahedra. There are key differences in the observed high pressure post-quartz crystalline structures of Kingma *et al.*[1(b)] and Haines *et al.*,[4] which probably stem from the different hydrostatic conditions and pathways adopted in the experiments.

First principles molecular dynamics simulations[7] predicted a trigonal structure for silica (space group $P3_2$) with two thirds of silicon atoms in octahedral coordination and one third which are 5-coordinated. The diffraction pattern of this phase compared well with the crystalline phase reported by Kingma *et al.*[1(b)] Due to the different approaches adopted, the post-quartz crystalline structures obtained by Wentzcovitch *et al.*[7] are different from those obtained in the present study. While our results involve structural optimization of the 9-atom quartz unit cell at high pressure and zero temperature, Wentzcovitch *et al.*[7] optimized the geometry of their 27-atom supercell while compressing it to 33 GPa and their resulting structure was annealed at temperatures fluctuating between 300–600 K for 0.8 ps followed by a rapid quench to 0 K.

Theoretical calculations using interatomic potentials to understand the high pressure post-quartz crystalline phases have also been reported.[12–14,16] Molecular-dynamics calculations[12] at $T = 300$ K reveal a crystalline-to-crystalline transition from α-quartz to a phase with a five-coordinated silicon structure at high pressure under nonhydrostatic conditions having the same space group as α-quartz. Various other low symmetry monoclinic structures[14,16] have also been obtained using the Tsuneyuki *et al.*[24] and van Beest *et al.*[25] interatomic potentials. Our studies reveal that while the simulations using interatomic potentials fitted to first principles energy surface give results in qualitative agreement with first principles, there are important differences. A possible reason for this discrepancy is the inability of isotropic pair potentials to accurately describe the zero pressure LO-TO splittings,[20(a)] and in consequence the complete phonon spectra of quartz.[20(a)] There are reported controversies[3,16] on the appropriate Born stability criteria adopted at high pressure and the reported mechanical instabilities at high pressure. Our studies however, are in qualitative agreement with the reported Brillouin scattering measurements of Gregoryanz *et al.*[3(a)] that suggest high pressure ferroelastic transitions in α-quartz driven by the violations of the Born stability criteria for B_3.

The monoclinic *C*2 structure we report as well as the various high pressure post-quartz structures reported by others[7,16] are interestingly racemic with chiral properties. The α-quartz structure features helices of corner-linked SiO_4 tetrahedra that can adopt either left- or right-handed configurations; the chiral behavior of quartz has aroused much interest.[53,54] Theoretical studies using interatomic potentials[16] indicate that while the high pressure monoclinic quartz II structure is ferroelastic in principle, the transition itself is coelastic, as the shape of the newly formed crystal is determined by the handedness of α-quartz. *Ab initio* studies of the energy barriers for switching the handedness in the high pressure monoclinic quartz structure are desirable, due to the differences between the interatomic potentials and first principles results.

Toledano and Machon[55] have explained the mechanism of amorphization under pressure of α-quartz and ice, and the microstructural properties of some ferroelectric relaxors based on a ferroelastic glass state that may form in crystalline material under the following conditions:[55] (i) the ferroelastic structure can exist in crystallographic configurations corresponding to different spontaneous strain components and (ii) an internal stress field is created involving the stress components conjugated to the preceding strains that induces sufficiently large mismatches between the differently sheared domains, leading to a splitting and disintegration of the mesoscopic-size domains into nanodomains, destroying the long-range order in the crystal. Ferroelastic behavior in the high pressure regime in α-quartz is indicated and is of interest, as spontaneous strains can lower the symmetry. All these materials including silica,[23] ice,[31] and some relaxors[56] seem to have a complex energy landscape with a soft energy surface and various competing energetically equivalent structures. It is interesting to contemplate whether competing high pressure ferroelastic phases can lead to a ferroelastic glass state in silica, which in turn leads to its amorphization. A microscopic understanding of the complex energy landscape in silica and the possible role of ferroelastic phases may perhaps provide more insight into the fundamental mechanisms of the observed high pressure amorphization.

V. CONCLUSIONS

High pressure first principles density functional theory calculations help us understand the role of phonon and elastic instabilities in the high pressure structural phase transitions and amorphization of α-quartz. Nonhydrostatic stresses are found to significantly influence the instabilities and explain the wide range of transition pressures observed in the experiments. A monoclinic high pressure post-quartz dense silica phase is obtained from structural relaxation in the vicinity of the K-point instability, in which two-thirds of the silicon atoms are in octahedral coordination. This $C2$ structure with effective silicon coordination intermediate between quartz and stishovite is metastable at ambient pressure. Possible links between the ferroelastic nature of high pressure silica transformations and pressure induced amorphization are outlined.

ACKNOWLEDGMENTS

[1] (a) K. J. Kingma, C. Meade, R. J. Hemley, H. K. Mao, and D. R. Veblen, Science **259**, 666 (1993); (b) K. J. Kingma, R. J. Hemley, H. K. Mao, and D. R. Veblen, Phys. Rev. Lett. **70**, 3927 (1993); (c) L. E. McNeil and M. Grimsditch, *ibid.* **72**, 1301 (1994).

[2] E. G. Ponyatovsky and O. I. Barkalov, Mater. Sci. Rep. **8**, 147 (1992).

[3] (a) E. Gregoryanz, R. J. Hemley, H.-K. Mao, and P. Gillet, Phys. Rev. Lett. **84**, 3117 (2000); (b) M. H. Muser and P. Schoffel, *ibid.* **90**, 079701 (2003); (c) E. Gregoryanz, R. J. Hemley, H. K. Mao, R. E. Cohen, and P. Gillet, *ibid.* **90**, 079702 (2003).

[4] J. Haines, J. M. Léger, F. Gorelli, and M. Hanfland, Phys. Rev. Lett. **87**, 155503 (2001).

[5] H. J. McSkimin, P. Andreatch, and R. N. Thurston, J. Appl. Phys. **36**, 1624 (1965).

[6] (a) L. E. McNeil and M. Grimsditch, Phys. Rev. Lett. **68**, 83 (1991); (b) W. Kittinger, J. Tichy, and E. Bertagnolli, *ibid.* **47**, 712 (1981); (c) N. Keskar and J. R. Chelikowsky, Nature (London) **358**, 222 (1992).

[7] R. M. Wentzcovitch, C. da Silva, J. R. Chelikowsky, and N. Bingelli, Phys. Rev. Lett. **80**, 2149 (1998).

[8] S. L. Chaplot and S. K. Sikka, Phys. Rev. B **47**, 5710 (1993).

[9] S. L. Chaplot and S. K. Sikka, Phys. Rev. Lett. **71**, 2674 (1993).

[10] S. L. Chaplot, Phys. Rev. Lett. **83**, 3749 (1999).

[11] J. S. Tse and D. D. Klug, Phys. Rev. Lett. **67**, 3559 (1991); J. S. Tse and D. D. Klug, *ibid.* **70**, 174 (1993); J. S. Tse, D. D. Klug, Y. Le Page, and M. Bernasconi, Phys. Rev. B **56**, 10878 (1997).

[12] J. Badro, D. M. Teter, R. T. Downs, P. Gillet, R. J. Hemley, and J.-L. Barrat, Phys. Rev. B **56**, 5797 (1997).

[13] J. Badro, J.-L. Barrat, and P. Gillet, Phys. Rev. Lett. **76**, 772 (1996); J. Badro, P. Gillet, and J.-L. Barrat, Europhys. Lett. **42**, 643 (1998).

[14] M. S. Somayazulu, S. M. Sharma, and S. K. Sikka, Phys. Rev. Lett. **73**, 98 (1994).

[15] N. Binggeli and J. R. Chelikowsky, Phys. Rev. Lett. **69**, 2220 (1992); N. Binggeli, N. R. Keskar, and J. R. Chelikowsky, Phys. Rev. B **49**, 3075 (1994).

[16] C. Campana, Martin H. Muser, J. S. Tse, D. Herzbach, and P. Schoffel, Phys. Rev. B **70**, 224101 (2004).

[17] S. Baroni and P. Gianozzi, in *High Pressure Materials Research*, edited by R. M. Wentzcovitch, R. J. Hemley, W. J. Nellis, and P. Y. Yu, Materials Research Society Proc. 499, Pittsburgh, 1998, p. 233.

[18] B. Holm and R. Ahuja, J. Chem. Phys. **111**, 2071 (1999).

[19] A. Trave, P. Tangney, S. Scandolo, A. Pasquarello, and R. Car, Phys. Rev. Lett. **89**, 245504 (2002); M. B. Smirnov and A. P. Mirgorodsky, *ibid.* **78**, 2413 (1997).

[20] (a) X. Gonze, D. C. Allan, and M. P. Teter, Phys. Rev. Lett. **68**, 3603 (1992); (b) X. Gonze, J. C. Charlier, D. C. Allan, and M. P. Teter, Phys. Rev. B **50**, 13035 (1994); (c) C. Lee and X. Gonze, *ibid.* **51**, 8610 (1995).

[21] C. Lee and X. Gonze, Phys. Rev. Lett. **72**, 1686 (1994); C. Lee and X. Gonze, Phys. Rev. B **56**, 7321 (1997).

[22] D. W. Dean, R. M. Wentzcovitch, N. Keskar, J. R. Chelikowsky, and N. Binggeli, Phys. Rev. B **61**, 3303 (2000).

[23] D. M. Teter, R. J. Hemley, G. Kresse, and J. Hafner, Phys. Rev.

Lett. **80**, 2145 (1998).

[24] S. Tsuneyuki, H. Aoki, M. Tsukada, and Y. Matsui, Phys. Rev. Lett. **64**, 776 (1990).

[25] B. W. H. van Beest, G. J. Kramer, and R. A. van Santen, Phys. Rev. Lett. **64**, 1955 (1990).

[26] E. Demiralp, T. Cagin, and W. A. Goddard, III, Phys. Rev. Lett. **82**, 1708 (1999).

[27] G. Dolino, P. Bastie, B. Capelle, V. Chamard, J. Hartwig, and P. L. Guzzo, Phys. Rev. Lett. **94**, 155701 (2005); F. Mogeon, G. Dolino, and M. Vallade, Phys. Rev. Lett. **62**, 179 (1989).

[28] (a) R. A. Angel, D. R. Allan, R. Miletich, and L. W. Finger, J. Appl. Crystallogr. **30**, 461 (1997); (b) L. Levien, C. T. Prewitt, and D. J. Weidner, Am. Mineral. **65**, 920 (1980); (c) J. Glinnemann, H. E. King, H. Schulz, Th. Hahn, S. J. La Placa, and F. Dacol, Z. Kristallogr. **198**, 177 (1992); (d) R. M. Hazen, L. W. Finger, R. J. Hemley, and H. K. Mao, Solid State Commun. **72**, 507 (1989); (e) W. G. Wyckoff, *Crystal Structures* (Interscience, New York, 1974).

[29] R. J. Hemley, in High Pressure Research in Mineral Physics, (edited by M. H. Manghnani and Y. Syono, Terra Scientific Publishing Company (TERRAPUB)/American Geophysical Union, Tokyo/Washington, D.C., 1987), p. 347.

[30] For a review, see R. J. Hemley, C. T. Prewitt, and K. J. Kingma, in *Silica: Physical Behavior, Geochemistry and Materials Applications*, Reviews in Mineralogy, edited by P. J. Heaney, C. T. Prewitt, and G. V. Gibbs, Mineralogical Society of America, Washington DC, 1994, Vol. 29, p. 41; D. Strauch and B. Dorner, J. Phys.: Condens. Matter **5**, 6149 (1993); H. Schober, D. Strauch, K. Nutzel, and B. Dorner, *ibid.* **5**, 6155 (1993).

[31] R. M. Wentzcovitch, *Proc. of CECAM Workshop on "Atomic structure and transport in glassy networks,"* (2002) (unpublished); K. Umemoto, R. M. Wentzcovitch, S. Baroni, and S. de Gironcoli, Phys. Rev. Lett. **92**, 105502 (2004); K. Umemoto, R. M. Wentzcovitch, S. Baroni, and S. de Gironcoli, Phys. Rev. B **69**, 180103(R) (2004).

[32] S. Baroni, S. de Gironcoli, A. D. Corsco, and P. Giannozzi, Rev. Mod. Phys. **73**, 515 (2001).

[33] S. Baroni, P. Giannozzi, and A. Testa, Phys. Rev. Lett. **58**, 1861 (1987); P. Giannozzi, S. de Gironcoli, P. Pavone, and S. Baroni, Phys. Rev. B **43**, 7231 (1991).

[34] M. C. Payne, M. P. Teter, D. C. Allan, T. A. Arias, and J. D. Joannopoulos, Rev. Mod. Phys. **64**, 1045 (1992).

[35] X. Gonze, Phys. Rev. B **54**, 4383 (1996).

[36] X. Gonze, Phys. Rev. B **55**, 10 337 (1997).

[37] X. Gonze and C. Lee, Phys. Rev. B **55**, 10 355 (1997).

[38] D. R. Hamann, X. Wu, K. M. Rabe, and D. Vanderbilt, Phys. Rev. B **71**, 035117 (2005); X. Wu, D. Vanderbilt, and D. R. Hamann, *ibid.* **72**, 035105 (2005).

[39] The ABINIT code is a collaborative project of the Universite Catholique de Louvain, Corning Inc. and other collaborators (URL: http://www.abinit.org/); X. Gonze, J.-M. Beuken, R. Caracas, F. Detraux, M. Fuchs, G.-M. Rignanese, L. Sindic, M. Verstraete, G. Zerah, F. Jollet, M. Torrent, A. Roy, M. Mikami, Ph. Ghosez, J.-Y. Raty, and D. C. Allan, Comput. Mater. Sci. **25**, 478 (2002).

[40] J. P. Perdew and A. Zunger, Phys. Rev. B **23**, 5048 (1981).

[41] D. M. Ceperley and B. J. Alder, Phys. Rev. Lett. **45**, 566 (1980).

[42] M. P. Teter (unpublished).

[43] B. B. Karki, L. Stixrude, and R. M. Wentzcovitch, Rev. Geophys. **39**, 507 (2001).

[44] L. Fast, J. M. Wills, B. Johansson, and O. Eriksson, Phys. Rev. B **51**, 17431 (1995).

[45] J. Wang, S. Yip, S. R. Phillpot, and D. Wolf, Phys. Rev. Lett. **71**, 4182 (1983); T. Barron and M. L. Klein, Proc. Phys. Soc. London **85**, 523 (1965).

[46] D. C. Wallace, Rev. Mod. Phys. **37**, 57 (1965); D. C. Wallace, *Thermodynamics of Crystals* (Wiley, New York, 1972).

[47] G. J. Ackland and S. K. Reed, Phys. Rev. B **67**, 174108 (2003).

[48] J. R. Chelikowsky, H. E. King, N. Troullier, J. Luis Martins, and J. Glinnemann, Phys. Rev. Lett. **65**, 3309 (1990).

[49] Th. Demuth, Y. Jeanvoine, J. Hafner, and J. G. Angyan, J. Phys.: Condens. Matter **11**, 3833 (1999).

[50] D. R. Hamann, Phys. Rev. Lett. **76**, 660 (1996).

[51] Z. Wu and R. E. Cohen, cond-mat/0508004, 2005 (unpublished).

[52] R. T. Downs and M. H. Wallace, Am. Mineral. **88**, 247 (2003).

[53] R. M. Hazen and D. S. Sholl, Nat. Mater. **2**, 367 (2003).

[54] R. T. Downs and R. M. Hazen, J. Mol. Catal. A: Chem. **216**, 273 (2004).

[55] P. Tolédano and D. Machon, Phys. Rev. B **71**, 024210 (2005).

[56] N. Choudhury, Z. Wu, E. J. Walter, and R. E. Cohen, Phys. Rev. B **71**, 125134 (2005); N. Choudhury, R. E. Cohen, and E. J. Walter, cond-mat/0508661 (unpublished).